ORIGINAL PAPER

CrossMark

Improved electrochemical performance of Li_2FeSiO_4/C as cathode for lithium-ion battery via metal doping

Ling Li[1] · Enshan Han[1] · Hui Liu[1] · Chen Mi[1] · YaKe Shi[1] · Xu Yang[1]

Abstract

$Li_2FeSi_{0.98}M_{0.02}O_4$/C (M = Ti, Ag, Cu, V, Pb) was synthesized as cathode material for lithium-ion battery by the solid-state method. The electrochemical performance of $Li_2FeSi_{0.98}M_{0.02}O_4$/C was investigated by constant current charge–discharge test, cyclic voltammetry (CV), and electrochemical impedance spectroscopy (EIS). The results show that the materials doped with Ti or Ag at the Si site deliver good initial discharge capacity. $Li_2FeSi_{1-x}M_xO_4$/C (M = Ti, Ag; x = 0.01, 0.02, 0.03, 0.05) was synthesized via the solid-state method. By comparing the electrochemical properties, it can be observed that $Li_2FeSi_{0.98}Ti_{0.02}O_4$/C and $Li_2FeSi_{0.98}Ag_{0.02}O_4$/C have good initial discharge capacity. The initial discharge capacity of $Li_2FeSi_{0.98}Ti_{0.02}O_4$/C is 164.1 mAh/ g, which is equivalent to 0.98 Li^+ deintercalation. The capacity of $Li_2Fe_{0.98}Ti_{0.02}Si_{O4}$/C is 155.8 mAh/g after 10 cycles under 0.1 C, and the capacity retention rate is 94.9%. The initial discharge capacity of $Li_2FeSi_{0.98}Ag_{0.02}O_4$/C is 166.6 mAh/g, which is better than other materials. The capacity of $Li_2Fe_{0.98}Ag_{0.02}Si_{O4}$/C is 132.8 mAh/g after 10 cycles under 0.1 C, and the capacity retention rate is 79.7%. The charge–discharge cycle performance of $Li_2FeSi_{0.98}Ti_{0.02}O_4$/C is more stable than $Li_2FeSi_{0.98}Ag_{0.02}O_4$/C. The Li^+ diffusion coefficient of $Li_2FeSi_{0.98}Ti_{0.02}O_4$/C is higher than that of pure phase material by two orders of magnitude. The $Li_2FeSi_{0.98}Ti_{0.02}O_4$/C and $Li_2FeSi_{0.98}Ag_{0.02}O_4$/C were tested by XRD and SEM. The XRD patterns show that there are no characteristic peaks of Fe or Li_2SiO_3 impurities in the materials, which indicates that the crystal structure of Li_2FeSiO_4 has not been changed after doping metal ion at the Si site. The SEM images indicate that the particle size of materials is quite uniform and no obvious agglomeration is detected in the materials. $Li_2FeSi_{0.98}Ti_{0.02}O_4$/C was analyzed by EDS, ICP, XPS, and FT-IR spectra since it delivers better performance when compared with other materials. EDS and ICP show that the values which were measured according to the ratio of each element are found to be similar to the theoretical values. The XPS spectrum confirms the existence of the characteristic peaks of Li, Fe, Si, and O in samples, which could also prove that Si^{4+} is successfully replaced by Ti^{4+} in the crystal structure of Li_2FeSiO_4. The position of each absorption peak in the infrared spectrogram coincides with that reported in the literatures, which indicates that the stable materials are formed.

Keywords Li_2FeSiO_4 · Ti, Ag doping · Solid-state method · Li-ion battery · Electrochemical performance

Introduction

Li_2FeSiO_4 is considered as one of the most promising cathode materials due to such advantages as high capacity, low price of raw materials, stable structure, and environmental benignity [1]. Such kinds of material also have excellent chemical, electrochemical, and thermal stability because of the strong bonding force in the structure. As the electron bandwidth of silicate is lower than that of phosphate, the former has higher electron conductivity. Therefore, polyanionic ferric silicate lithium has great potential to become a new generation of cathode material for lithium-ion battery. Compared with $LiCoO_2$, $LiNiO_2$, and $LiMn_2O_4$, Li_2FeSiO_4 can have not only the advantages mentioned above, but also the ability of intercalating two lithium ions theoretically, which could increase the theoretical capacity as high as 332 mAh/g [2]. Thanks to the properties listed in this paragraph, the ferrous lithium silicate cathode materials rapidly attract lots of attention from researchers worldwide.

✉ Ling Li
537742870@qq.com

✉ Enshan Han
eshan@hebut.edu.cn

[1] School of Chemical Engineering and Technology, Hebei University of Technology, Tianjin 300130, People's Republic of China
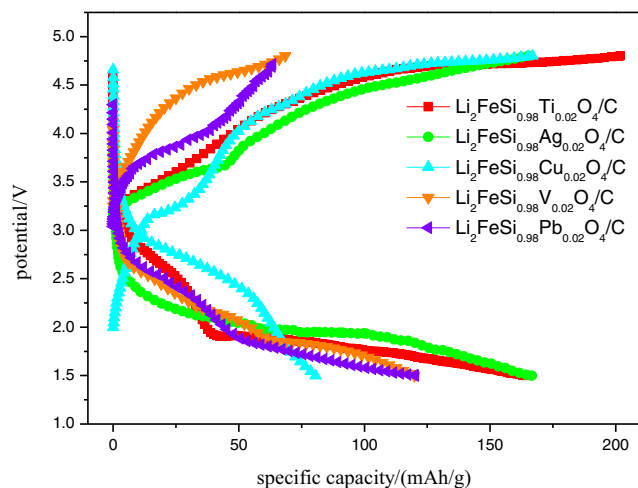
Fig. 1 Initial charge/discharge curves of $Li_2FeSi_{0.98}M_{0.02}O_4$/C at 0.1 C

Fig. 3 The cyclic voltammetry of $Li_2FeSi_{0.98}M_{0.02}O_4$/C

The reported methods for the synthesis of Li_2FeSiO_4 include the solid-phase method [3], sol–gel method [4–6], and hydrothermal method [7, 8]. The solid-phase method has the advantages of simple preparation process and easy industrialization. Ren Bing et al. [9] prepared Li_2FeSiO_4 by the solid-phase method. The charging and discharging test was performed at the current density of 0.1 C at room temperature with voltage between 1.5 and 4.8 V. The initial discharge capacity showed about 170 mAh/g, which indicated that the material had a good electrochemical performance. Compared with the solid-phase method, the sol–gel method has the advantages of uniform distribution, small particle size, and easy reaction control, but the process of synthesis is complicated and time consuming. S. Zhang et al. [10] used citric acid as carbon source and complex agent to synthesize Li_2FeSiO_4/C. The maximum discharge capacity was measured at 153.6 mAh/g under the condition of C/16 multiplier, 1.5–4.8 V. After 80 cycles, the capacity retention could reach 98.3%. Pure phase materials are easy to produce via the
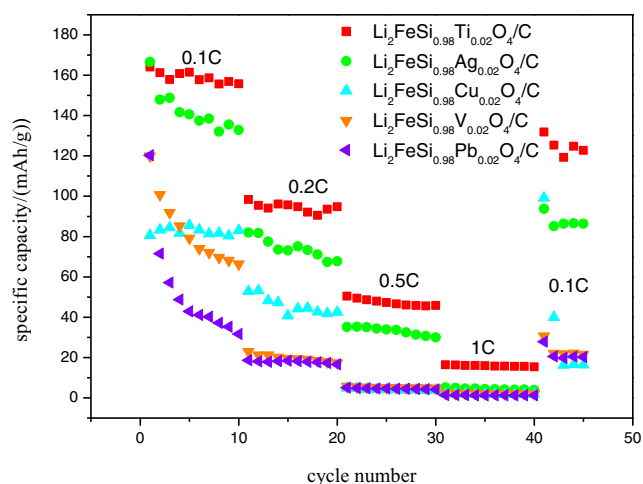
hydrothermal method, but it is costly and difficult to conduct and relies on the experimental equipment. Gong et al. [11] synthesized Li_2FeSiO_4 samples by hydrothermal method with the multiplier of C/16, and the initial discharge capacity was measured 160 mAh/g.

Although 1 Li^+ can be deintercalated from Li_2FeSiO_4 to reach the theoretical capacity of 166 mAh/g, the low electronic conductivity and Li^+ mobility could lead to the poor multiplier performance, which limits its broad application. In order to overcome those difficulties and improve the electrochemical performance of Li_2FeSiO_4, the following improvements are adopted recently: (1) Reduce the particle size and improve the purity of materials. The lithium-ion migration distance could be shortened by reducing the particle. The electrochemical properties of the material could be improved by increasing the purity. Z.L. Tao et al. [12] synthesized the porous Li_2FeSiO_4/C. Charging and discharging tests were carried out in the voltage range of 1.5–4.8 V with the magnification of 0.5 C. Results showed that the initial discharge capacity of the material was 176.8 mAh/g. (2) Carbon coating is also a common way to improve the properties of Li_2FeSiO_4 materials. This method can not only improve the conductivity of materials, but also effectively inhibit the growth of particles. In 2012, L. Qu et al. [5] synthesized Li_2FeSiO_4/C cathode materials by the sol–gel method. During the synthesis, sucrose was used as carbon source. The initial discharge capacity of the material was 140 mAh/g, which was measured at 0.1 C. After that, the capacity of the material kept increasing and was basically stable at 160 mAh/g after 50 cycles. (3) Doping ionic [13–15]. Lattice defects could be caused by doping ionic which could improve the conductivity and charge–discharge capacity of material. S. Zhang et al. succeeded in synthesizing $Li_2Fe_{0.97}Mg_{0.03}SiO_4$ [16], $Li_2Fe_{0.97}M_{0.03}SiO_4$ (M = Zn^{2+}, Cu^{2+}, Ni^{2+}) [15], and

Fig. 2 Cyclic performance of $Li_2FeSi_{0.98}M_{0.02}O_4$/C at different rates

Fig. 4 Electrochemical impedance spectroscopy (EIS) of $Li_2FeSi_{0.98}M_{0.02}O_4/C$
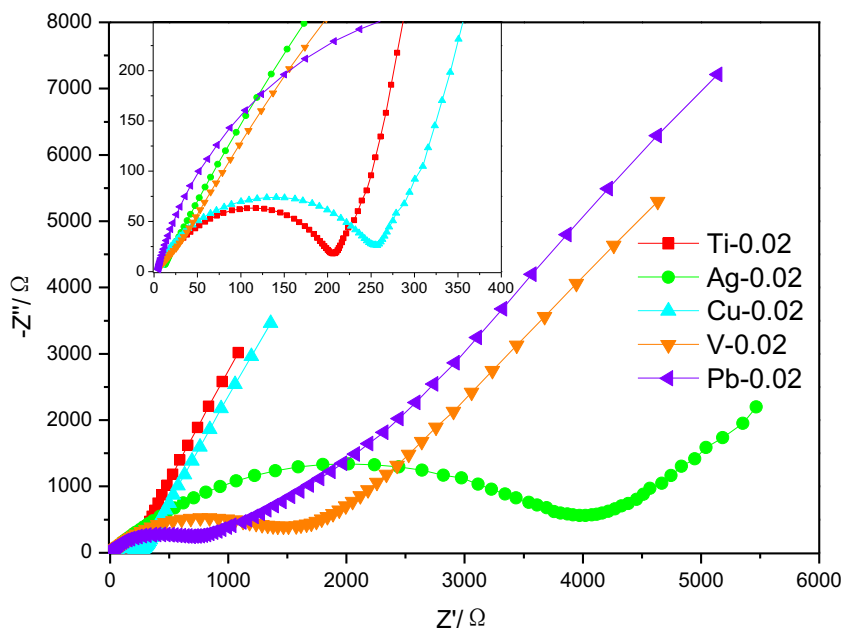
$Li_2Fe_{1-x}Cr_xSiO_4$ [17]. The results showed that Mg and Zn were successfully doped into Li_2FeSiO_4 material, and the cyclic stability of the material was improved since the crystal structure of the material was fixed. The initial discharge capacity of $Li_2Fe_{0.97}Cr_{0.03}SiO_4$ was 158 mAh/g at C/16 with the voltage range of 1.5–4.6 V, and the capacity was almost unchanged after the 20th cycle. It indicates that the material exhibits high reversible capacity and good multiplying performance. Chen MR et al. [18] synthesized $Li_{2.06}FeSiO_4F_{0.02}/C$ cathode materials by hydrolysis-step calcination process. The initial discharge capacity of the material was 116.8 mAh/g under 0.3 C at 55 °C. M.E. Arroyo-de Dompablo [19] explained the influence of the replacement of O by N or F on the electrochemical properties of new materials from the theoretical perspective. Due to the oxidation reaction of N^{3-}, the doping of N does not affect the capacity of the material, while the F always combines with the active transition metal ions, which leads to the reduction of the specific capacity and weakens the electrochemical properties of the material finally.

In this paper, $Li_2FeSi_{0.98}M_{0.02}O_4/C$ (M = Ti, Ag, Cu, V, and Pb) materials have been synthesized by the solid-state method. The electrochemical performance was tested by constant current charge–discharge, cyclic voltammetry, and

electrochemical impedance spectroscopy. The better kinds of doping metals are selected according to the experimental results. Subsequently, $Li_2FeSi_{1-x}M_xO_4/C$ (M = Ti, Ag; x = 0.01, 0.02, 0.03, 0.05) was synthesized, and the electrochemical properties were tested and analyzed. The electrochemical properties of the materials doped in different proportions with the same metal were investigated to obtain the optimal metal type and doping ratio. Then, the selected materials were characterized and analyzed by XRD, SEM, EDS, ICP, XPS, and FT-IR.

Experimental

Synthesis of the cathode material

$Li_2FeSi_{0.98}M_{0.02}O_4/C$ (M = Ti, Ag, Cu, V, and Pb) and $Li_2FeSi_{1-x}M_xO_4/C$ (M = Ti, Ag; x = 0.01, 0.02, 0.03, 0.05) were synthesized as follows. The lithium source (CH_3COOLi), iron source ($FeC_2O_4 \cdot 2H_2O$), silicon source (TEOS), carbon source (citric acid), and doping metal source (TiO_2, CH_3COOAg, $Cu(CH_3COO)_2 \cdot H_2O$, V_2O_5, $Pb(CH_3COO)_2 \cdot 3H_2O$) were taken in proportion and placed in the ball mill tank. Before ball milling, about 10 ml anhydrous alcohol was added as medium. After that, the mixture was milled at the speed of 250 r/min for 5 h. Then, that mixture was dried at 80 °C in a vacuum oven and ground in a glove box filled with high purity Ar for 20 min. After that, the powder was preheated in a tube furnace under N_2 atmosphere, at 350 °C for 5 h. Then, it was ground again about 30 min after cooling. Finally, the precursor powder was calcined under N_2 atmosphere at 700 °C for 10 h, and the materials were obtained after natural cooling.
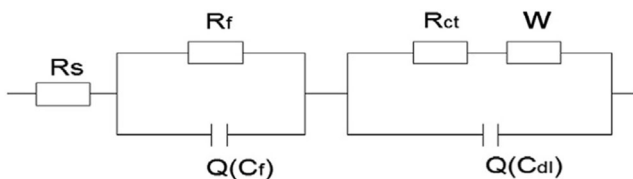

Fig. 5 Equivalent circuit for fitting of EIS

Table 1 EIS fitting data of $Li_2FeSi_{0.98}M_{0.02}O_4/C$

Samples	R_s (Ω)	Q (C_f) (F)	R_f (Ω)	Q (C_{dl}) (F)	R_{ct} (Ω)	$W/Ω/s^{1/2}$	σ	D_{Li}^+ (cm² s⁻¹)
$Li_2FeSi_{0.98}Ti_{0.02}O_4/C$	2.59	1.58×10^{-5}	212.2	2.65×10^{-3}	217	7.23×10^{-3}	169.11	1.32×10^{-15}
$Li_2FeSi_{0.98}Ag_{0.02}O_4/C$	8.914	2.499×10^{-3}	1440	1.42×10^{-5}	4.24×10^3	5.76×10^4	244.16	6.34×10^{-16}
$Li_2FeSi_{0.98}Cu_{0.02}O_4/C$	3.294	1.280×10^{-5}	257.2	2.15×10^{-3}	8.28×10^4	5.589	205.48	8.95×10^{-16}
$Li_2FeSi_{0.98}V_{0.02}O_4/C$	3.186	1.230×10^{-5}	1178	7.44×10^{-5}	70.91	5.91×10^{-4}	496.91	1.53×10^{-16}
$Li_2FeSi_{0.98}Pb_{0.02}O_4/C$	10.180	1.040×10^{-5}	1734	1.09×10^{-3}	6123	1.21×10^{-4}	426.52	2.08×10^{-16}

Preparation of positive film and battery assembly

The active material, polyvinylidene fluoride (PVDF), and conductive carbon black were taken by a mass ratio of 8:1:1, and dissolved in the *N*-methyl-pyrrolidone (NMP). The aluminum foil was covered over by that slurry and then the electrode film was dried at 110 °C for 10 h. After that, the electrode film was pressed and punched into a circular disc, and the cathode electrodes were made. The CR2032 coin cell was used to test the electrochemical properties of the cathode electrodes mentioned above. The cell was made of a lithium metal electrode with a polypropylene microporous film (Celgard2300) in the middle. The $LiPF_6$ (1 M) was used as electrolyte in ethylene carbonate (EC), dimethyl carbonate (DMC), and ethyl methyl carbonate (EMC), while the coin cells were installed in a glove compartment where the relative humidity is less than 4%.

Electrochemical and material characterization

In this experiment, Land CT2001A was used to test the electrochemical performance with the voltage ranging from 1.5 to 4.8 V. Cyclic voltammetry and electrochemical impedance measurements were performed on a CHI660C electrochemical analyzer, and the voltage range of CV was 1.7–4.0 V (versus Li^+/Li) with a scanning rate of 0.1 mV s⁻¹. The frequency range of the electrochemical impedance spectroscopy (EIS) was set from 100 kHz to 0.01 Hz, while the AC amplitude was 5 mV. The software ZsimpWin 3.10 was used to analyze the EIS data. Crystal structure of the materials was represented by X-ray diffraction (XRD) analyzer (D8-Fouse, made in Germany) with Cu-Kα radiation. The scanning range was 10–80° while the scanning speed was 12°/min. The morphologies of the powders were analyzed by scanning electron microscope
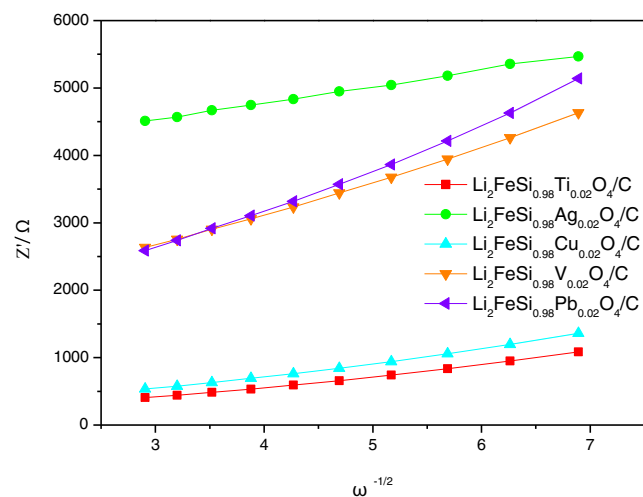
Fig. 6 Linear fitting of the Z′ versus $\omega^{-1/2}$ relationship of $Li_2FeSi_{0.98}M_{0.02}O_4/C$

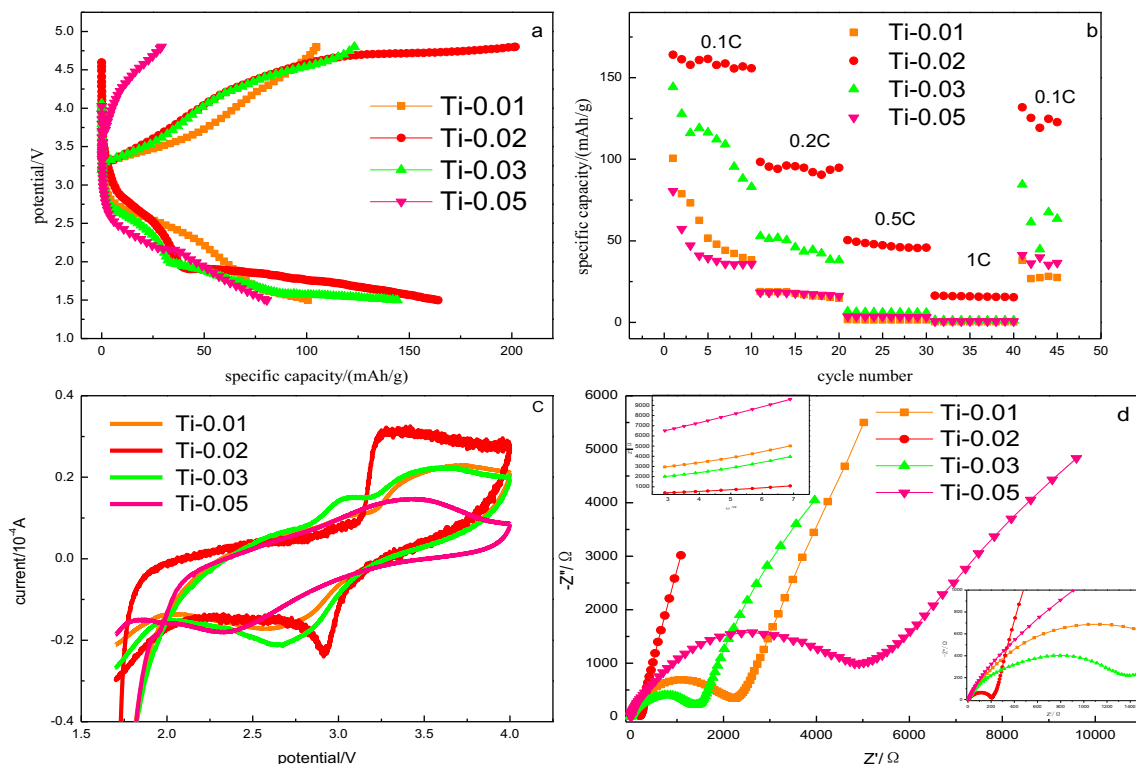**Fig. 7** Electrochemical performance diagram of $Li_2FeSi_{1-x}Ti_xO_4/C$ (the initial charge/discharge curves (**a**), cyclic performance at different rates (**b**), the cyclic voltammetry (**c**), and electrochemical impedance spectroscopy (**d**))

(SEM, Nova Nano SEM 450 FEI). The species and distribution of elements which is on the surface of the sample can be obtained by an energy dispersive spectrometer (EDS, AMETE, and OCTANE PLUS, made in America). The composition of metal elements in the sample was determined by inductively coupled plasma emission spectrometer (inductively coupled plasma-optical emission spectrometer, ICP-OES). The iCAP6300 instrument produced by Thermo Company of USA was used. The X-ray photoelectron spectroscopy (XPS, Thermo Fisher Scientific, and ESCALAB250Xi, made in America) was used to analyze the materials, then the species and chemical states of the atoms were recognized. By using Fourier-transform infrared spectrometer (FT-IR, BRUKER, and TENSOR27, made in German), the functional groups in the materials can be identified.

Results and discussion

Electrochemical characteristics of $Li_2FeSi_{0.98}M_{0.02}O_4/C$

The initial charge/discharge curves of $Li_2FeSi_{0.98}M_{0.02}O_4/C$ (M = Ti, Ag, Cu, V, and Pb) at 0.1 C are shown in Fig. 1. Figure 2 shows the graph of the cyclic performance curves, in which the data of the material cycles 10 times at the rates of 0.1 C, 0.2 C, and 0.5 C, and then 5 times at the rate of 0.1 C again. According to Fig. 1, the discharge platforms of $Li_2FeSi_{0.98}Ti_{0.02}O_4/C$ and $Li_2FeSi_{0.98}Ag_{0.02}O_4/C$ are obvious, and the initial discharge capacity shows 164.1 and 166.6 mAh/g, respectively, which is equivalent to 0.98 Li^+ and 1 Li^+ deintercalation. The cycling performance of $Li_2FeSi_{0.98}Cu_{0.02}O_4/C$ material is also relatively stable, but its capacity is low, and the initial discharge capacity shows

Table 2 EIS fitting data of $Li_2FeSi_{1-x}Ti_xO_4/C$

Samples	R_s (Ω)	Q (C_f) (F)	R_f (Ω)	Q (C_{dl}) (F)	R_{ct} (Ω)	$W/\Omega/s^{1/2}$	σ	D_{Li}^+ (cm^2 s^{-1})
$Li_2FeSi_{0.99}Ti_{0.01}O_4/C$	6.445	3.61×10^{-3}	1.22×10^4	9.7×10^{-4}	2.15×10^3	1.376×10^{-3}	515	1.42×10^{-16}
$Li_2FeSi_{0.98}Ti_{0.02}O_4/C$	2.59	1.58×10^{-5}	212.2	2.65×10^{-3}	217	7.23×10^{-3}	169.11	1.32×10^{-15}
$Li_2FeSi_{0.97}Ti_{0.03}O_4/C$	2.869	1.12×10^{-5}	1.371×10^3	1.256×10^{-3}	8.29×10^3	3.68×10^3	485.33	1.60×10^{-16}
$Li_2FeSi_{0.95}Ti_{0.05}O_4/C$	5.709	8.11×10^{-3}	2.89×10^3	4.21×10^{-4}	4.69×10^3	5.38×10^{-4}	773.1	6.32×10^{-17}
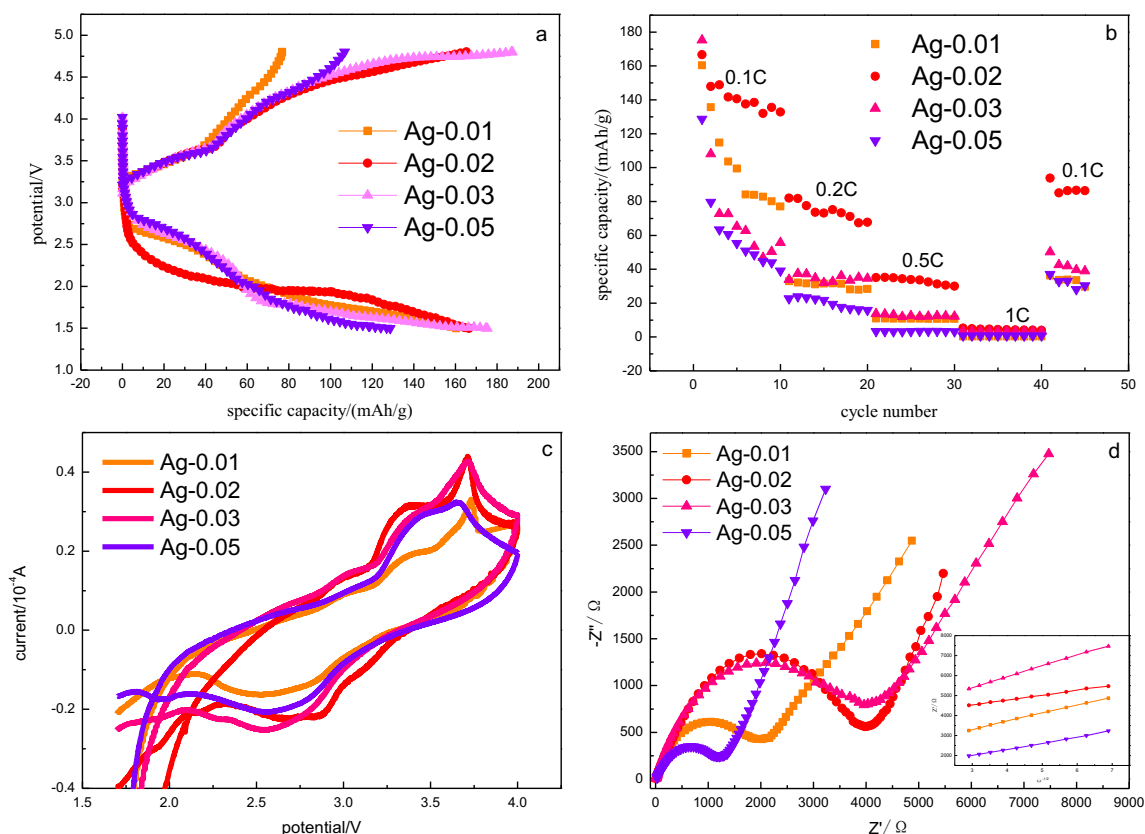
Fig. 8 Electrochemical performance diagram of $Li_2FeSi_{1-x}Ag_xO_4/C$ (the initial charge/discharge curves (**a**), cyclic performance at different rates (**b**), the cyclic voltammetry (**c**), and electrochemical impedance spectroscopy (**d**))

only 80.6 mAh/g. The initial charge–discharge capacity of the materials doped with V and Pb is not high, and the capability attenuates easily. It is mainly because that the metal which is doped in the cathode material hinders the deintercalation of Li^+, and the capacity is determined by both the amount of deintercalation of Li^+ and the speed of migration [20]. Therefore, the capacity of the materials doped with V and Pb is low, but higher than that of the pure phase Li_2FeSiO_4/C synthesized under the same experimental conditions [21]. Figure 2 indicates that the capacity is more stable at 0.2 C, 0.5 C, and 1 C. It is due to the Li^+ and Fe^{2+} rearrangement in the lattice of Li_2FeSiO_4 during the first charge and discharge cycle which results in the formation of a more stable structure of the Li_2FeSiO_4 lattice [22]. When the grain size of Li_2FeSiO_4 is reduced to nanoscale (< 100 nm), all of the ion rearrangements can be realized in a single charge/discharge

process. However, due to the large grain size and the large resistance of ion rearrangement, the Li_2FeSiO_4 materials synthesized by the solid-state method make it difficult to achieve ion rearrangement in one charge/discharge cycle. In order to achieve the most stable Li_2FeSiO_4 structure, multiple charge/discharge processes are required. The results show that the structure of the cathode material is relatively stable after 10 cycles at 0.1 C. It can be observed from Fig. 2 that the discharge capacity of $Li_2FeSi_{0.98}Ti_{0.02}O_4/C$ is higher than that of other materials at each rate, and the capacity retention rate is the best at each rate. Figure 2 shows the materials doped with Ti and Ag have better first discharge capacity. The capacity of $Li_2Fe_{0.98}Ti_{0.02}SiO_4/C$ shows 155.8 mAh/g after 10 cycles under 0.1 C, and the capacity retention rate is 94.9%. The capacity of $Li_2Fe_{0.98}Ag_{0.02}SiO_4/C$ reaches 132.8 mAh/g after 10 cycles under 0.1 C, and the capacity retention rate is 79.7%.

Table 3 EIS fitting data of $Li_2FeSi_{1-x}Ag_xO_4/C$

Samples	R_s (Ω)	Q (C_f) (F)	R_f (Ω)	Q (C_{dl}) (F)	R_{ct} (Ω)	$W/\Omega/s^{1/2}$	σ	D_{Li}^+ (cm^2 s^{-1})
$Li_2FeSi_{0.99}Ag_{0.01}O_4/C$	6.189	3.189×10^{-3}	590.5	1.23×10^{-5}	1.98×10^3	1.086×10^{-3}	404.69	2.31×10^{-16}
$Li_2FeSi_{0.98}Ag_{0.02}O_4/C$	8.914	2.499×10^{-3}	1440	1.42×10^{-5}	4.24×10^3	5.76×10^4	244.16	6.34×10^{-16}
$Li_2FeSi_{0.97}Ag_{0.03}O_4/C$	6.292	9.74×10^{-7}	3.527	9.06×10^{-6}	3.89×10^3	7.08×10^{-4}	541.56	1.29×10^{-16}
$Li_2FeSi_{0.95}Ag_{0.05}O_4/C$	15.91	3.20×10^{-5}	1344	1.49×10^{-3}	2.43×10^3	1.60×10^{-7}	309.98	3.93×10^{-16}
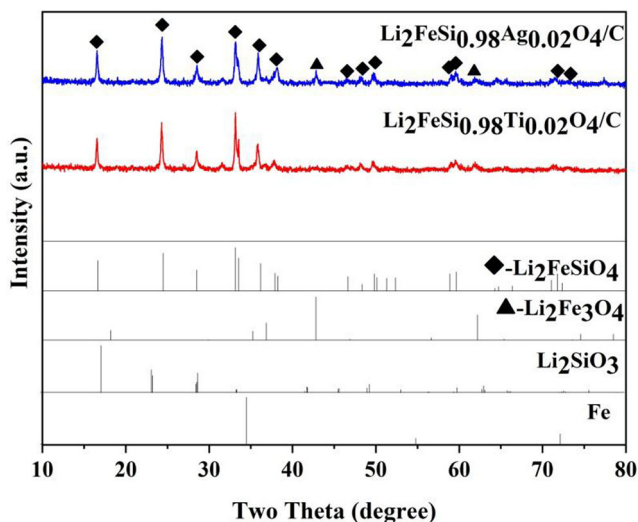
Fig. 9 XRD patterns of $Li_2FeSi_{0.98}Ti_{0.02}O_4$/C and $Li_2FeSi_{0.98}Ag_{0.02}O_4$/C

Therefore, through the results of the initial charge/discharge and cyclic performance, the appropriate doping metals are Ti and Ag.

Figure 3 shows cyclic voltammetry for the $Li_2FeSi_{0.98}M_{0.02}O_4$/C (M = Ti, Ag, Cu, V, and Pb). The redox peaks of $Li_2FeSi_{0.98}Ti_{0.02}O_4$/C and $Li_2FeSi_{0.98}Ag_{0.02}O_4$/C are large. There is a sharp peak in the oxidation peak of $Li_2FeSi_{0.98}Ag_{0.02}O_4$/C in the range of 3.5~3.8 V, which indicates that the Ag ion has successfully entered the lattice of the material and more lithium ions have escaped. The migration path of Li^+ is related to the crystal structure of the sample. The coulomb repulsion force exists between the oxygen atoms in the Li_2FeSiO_4 crystal lattice. The coulomb repulsion force leads to the change of the bond distance of the Fe–O, but the Si–O bond is extremely firm which guarantees the stability of the crystal lattice in the multiple charge and discharge cycles. In the process of the Li^+ deintercalation, the change of the Fe–O is larger than that of Si–O. After Ag doping, the Ag atom will replace the Fe atom. In the charging process, when Li^+ is deintercalated, the Fe^{2+} will be totally oxidized to Fe^{3+}. When Li^+ is further deintercalated, Ag^+ could not be oxidized to a higher valence state, but charge fluctuation will occur on the Ag–O bond which could lead to the instability of the structure of Li_2FeSiO_4. So, in the CV diagram, the current value of the oxidation peak located from 2.0 to 2.5 V changes rapidly. The reason is that the highest value state of the Ag leads to the instability of the total charge of the material. After charge and discharge cycles, the rearrangement of ions makes the crystal structure change from metastable to steady state, which ensures the stable cycle performance. The redox peak of $Li_2FeSi_{0.98}Cu_{0.02}O_4$/C is smaller than $Li_2FeSi_{0.98}Ti_{0.02}O_4$/C and the capacity of $Li_2FeSi_{0.98}Cu_{0.02}O_4$/C is lower when combined with Fig. 2. The electrochemical properties of the materials doped with V and Pb are poor, the peak line is not sharp, and the distance between peaks is larger. According to the data of Figs. 1 and 2, the conclusion could be made that the electrochemical properties of these materials are poor.

Figure 4 shows the AC impedance diagram of $Li_2FeSi_{0.98}M_{0.02}O_4$/C. The electrochemical impedance diagram can reveal the relationship between the measured potential and alternating currents. The resistance and charge transfer reactions of the solution are relevant to the migration of Li^+ and Li_2FeSiO_4 could also be affected by the migration of Li^+. Therefore, the internal resistance of the battery and the difficulty of lithium-ion migration can be analyzed with the help of the EIS diagram. The results show that doping metal atoms has a significant effect on the impedance. All EIS curves of $Li_2FeSi_{0.98}M_{0.02}O_4$/C are fitted with an equivalent circuit composed of "R (QR)(Q (RW))" (in Fig. 5) by using the ZSimpWin program, and the fitting results are shown in Table 1. Here, R_s, R_f, and R_{ct} are resistances of the electrolyte, the interface electric resistance, and the charge transfer reaction, respectively. The SEI film capacitance and the double layer capacitance are represented by the constant phase elements Q (C_f) and Q (C_{dl}), and the quasi-straight line at the low-frequency region represents the Warburg impedance (W) which is related to the impedance of Li^+ diffusion in bulk material.

$$D_{Li^+} = \frac{R^2 T^2}{2A^2 n^2 F^4 C^2 \sigma^2} \tag{1}$$

The linear fitting of Z' versus $\omega^{-1/2}$ in the low-frequency region of $Li_2FeSi_{0.98}M_{0.02}O_4$/C is shown in Fig. 6. The lithium-ion diffusion coefficients (D_{Li+}) of $Li_2FeSi_{0.98}M_{0.02}O_4$/C are calculated according to the equivalent circuit and lithium-ion diffusion coefficients: Eq. (1) [23], where R is the gas constant (8.314 J mol^{-1} K^{-1}), T is the absolute temperature, A is the surface area of the cathode (here, A was estimated to be the surface area of electrode, 0.785 cm^2), n is the number of electrons per molecule during

Table 4 Lattice parameters of $Li_2FeSi_{0.98}Ti_{0.02}O_4$/C and $Li_2FeSi_{0.98}Ag_{0.02}O_4$/C

y	a/(Å)	b/(Å)	c/(Å)	β (°)	V (Å^3)
$y = 0$	8.2349415	5.0067280	8.2239445	98.88957	334.65253
$Li_2FeSi_{0.98}Ti_{0.02}O_4$/C	8.2332958	5.010971	8.237078	98.87443	335.7673
$Li_2FeSi_{0.98}Ag_{0.02}O_4$/C	8.2377998	5.008369	8.236885	98.88287	335.7609
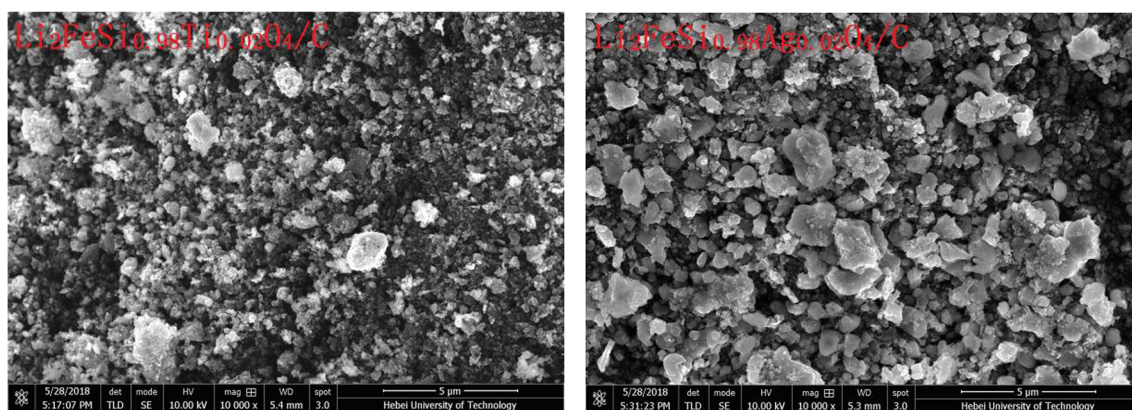
Fig. 10 SEM images of $Li_2FeSi_{0.98}Ti_{0.02}O_4/C$ and $Li_2FeSi_{0.98}Ag_{0.02}O_4/C$

oxidation, F is the Faraday constant (96,485.33 C mol^{-1}), C is the bulk concentration of Li$^+$ in the electrode (0.0390 mol cm^{-3} for Li_2FeSiO_4 [12]), and σ is the Warburg factor (the rake ratio of Fig. 6). The calculated results are shown in Table 1, that the diffusion coefficient of lithium ion increases obviously after doping metal ions. The lithium-ion diffusion coefficient of pure phase material is 1.842×10^{-17} [21]. After being doped, the lithium-ion diffusion coefficient of $Li_2FeSi_{0.98}Ti_{0.02}O_4/C$ increases by two orders of magnitude. At the same time, the R_{ct} of $Li_2FeSi_{0.98}Ti_{0.02}O_4/C$ is very small, which indicates that the material has high specific capacity and better cycling performance [7]. The lithium-ion diffusion coefficient of $Li_2FeSi_{0.98}Cu_{0.02}O_4/C$ is increased by an order of magnitude, but its R_{ct} is 8.28×10^4, which affects the charge–discharge performance of the material. The R_f of $Li_2FeSi_{0.98}Ag_{0.02}O_4/C$ is larger, so the initial discharge capacity is lower than that of $Li_2FeSi_{0.98}Ti_{0.02}O_4/C$. The R_{ct} of $Li_2FeSi_{0.98}Pb_{0.02}O_4/C$ is relatively large, so its electrochemical performance is also poor. The diffusion coefficient of lithium ion of the materials doped with V is better than that of pure phase material, which indicates that doping metal ions can improve the impedance performance of the materials.

Through the above analysis, it can be concluded that when M = Ti and Ag, the $Li_2FeSi_{0.98}M_{0.02}O_4/C$ materials synthesized by the solid-state method have a good electrochemical performance in charge/discharge capacity, rate performance, cyclic voltammetry, and AC impedance. Therefore, those two kinds of doped metal were chosen as the experimental subjects for the further experiment in which the optimum doping ratio could be identified. $Li_2FeSi_{0.99}M_{0.01}O_4/C$, $Li_2FeSi_{0.98}M_{0.02}O_4/C$, $Li_2FeSi_{0.97}M_{0.03}O_4/C$, and $Li_2FeSi_{0.95}M_{0.05}O_4/C$ (M = Ti and Ag) were synthesized and their electrochemical properties were tested and analyzed.

Electrochemical characteristics of $Li_2FeSi_{1-x}Ti_xO_4/C$

Figure 7 shows the initial charge/discharge curves, cyclic performance at different rates, cyclic voltammetry, and electrochemical impedance spectroscopy of $Li_2FeSi_{1-x}Ti_xO_4/C$ ($x = 0.01, 0.02, 0.03, 0.05$). From Fig. 7 a, we can observe that there are obvious discharge platforms in the initial charge–discharge diagram of $Li_2FeSi_{0.98}Ti_{0.02}O_4/C$ and $Li_2FeSi_{0.97}Ti_{0.03}O_4/C$. The initial discharge capacities are 100.6 mAh/g, 164.1 mAh/g, 144.3 mAh/g, and 80.5 mAh/g when $x = 0.01, 0.02, 0.03$, and 0.05, respectively. The initial discharge capacity of $Li_2FeSi_{0.98}Ti_{0.02}O_4/C$ corresponds to the deintercalation of 0.98Li$^+$. Figure 7 b indicates that the capacity attenuates seriously except $Li_2FeSi_{0.98}Ti_{0.02}O_4/C$. From the CV diagram, it can be observed that the peak area of $Li_2FeSi_{0.98}Ti_{0.02}O_4/C$ is the largest, and the potential difference between the two peaks is the smallest which is about
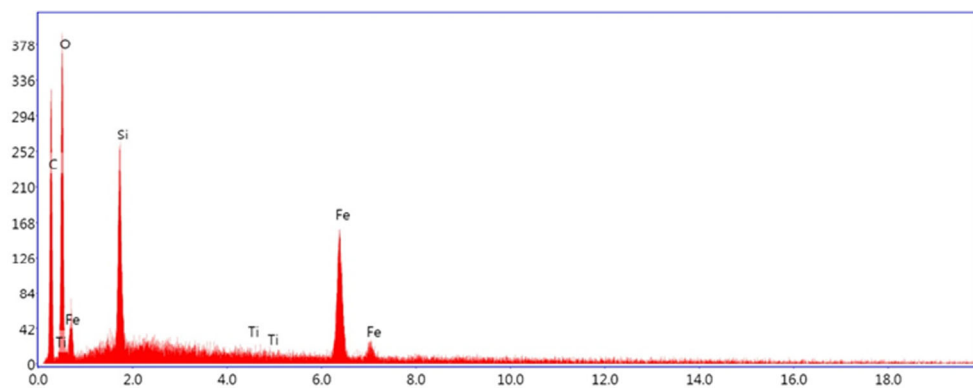
Fig. 11 EDS spectra of $Li_2FeSi_{0.98}Ti_{0.02}O_4/C$

Table 5   ICP-OES results of $Li_2FeSi_{0.98}Ti_{0.02}O_4$/C

Theoretical chemical formula	Measured atomic ratio				
	Li	Fe	Si	Ti	O
$Li_2FeSi_{0.98}Ti_{0.02}O_4$	2.000	1.003	0.978	0.019	4.010

0.3 V. It shows that $Li_2FeSi_{0.98}Ti_{0.02}O_4$/C delivers better charge–discharge capacity. Therefore, 0.02 is considered as the optimum doping ratio of Ti. The R_{ct} of $Li_2FeSi_{0.98}Ti_{0.02}O_4$/C in Table 2 is the smallest and the diffusion coefficient of Li^+ is two orders of magnitude higher than that of $Li_2FeSi_{0.95}Ti_{0.05}O_4$/C. It shows that the diffusion coefficient of lithium ion will be decreased when the doping ratio of Ti is too high. The proper amount of Ti doping reduces the charge transfer resistance of the cathode material during charge and discharge, increases the electronic conductivity of the material, and improves the electrochemical performance of the material. Combined with the above electrochemical performance analysis, it can be concluded the performance of $Li_2FeSi_{0.98}Ti_{0.02}O_4$/C is superior.

Electrochemical characteristics of $Li_2FeSi_{1-x}Ag_xO_4$/C

Figure 8 shows the initial charge/discharge curves, cyclic performance at different rates, cyclic voltammetry, and electro-chemical impedance spectroscopy of $Li_2FeSi_{1-x}Ag_xO_4$/C ($x = 0.01, 0.02, 0.03, 0.05$). Figure 8 a shows that the initial discharge specific capacity is 160.4 mAh/g, 166.6 mAh/g, 175.3 mAh/g, and 128.7 mAh/g when $x = 0.01, 0.02, 0.03,$ and 0.05, respectively. Figure 8 b indicates that when the Ag content increases, the capacity of the material attenuates seriously, but the capacity of $Li_2FeSi_{0.98}Ag_{0.02}O_4$/C is higher than

that of other materials at each ratio. Figure 8 c shows that the oxidation peaks of the materials doped with Ag are sharp at about 3.7 V. The peak area of $Li_2FeSi_{0.98}Ag_{0.02}O_4$/C is the largest and the distance between peaks is the shortest, which indicates that the material is stable. Combined with EIS curve fitting, it can be concluded that the lithium-ion diffusion co-efficient of the material is the largest. However, the R_{ct} of $Li_2FeSi_{0.95}Ag_{0.05}O_4$/C in Table 3 is higher than that of $Li_2FeSi_{0.99}Ag_{0.01}O_4$/C and $Li_2FeSi_{0.97}Ag_{0.03}O_4$/C. Combined with Fig. 8 b, the capacity attenuation of $Li_2FeSi_{0.95}Ag_{0.05}O_4$/C is higher than that of $Li_2FeSi_{0.99}Ag_{0.01}O_4$/C and $Li_2FeSi_{0.97}Ag_{0.03}O_4$/C. In summary, it can be concluded that when the Ag doping ratio is 0.02, the initial charge and discharge performance of the material is great and the performance of $Li_2FeSi_{0.98}Ag_{0.02}O_4$/C is stable.

Characterization and analysis of $Li_2FeSi_{0.98}Ti_{0.02}O_4$/C and $Li_2FeSi_{0.98}Ag_{0.02}O_4$/C

Through the analysis of the initial charge/discharge curves, cyclic performance at different rates, cyclic voltammetry, and electrochemical impedance spectroscopy, we know that $Li_2FeSi_{0.98}Ti_{0.02}O_4$/C and $Li_2FeSi_{0.98}Ag_{0.02}O_4$/C have good initial discharge capacity. Therefore, we will do further characterization analysis upon those two materials.

XRD patterns of the two samples are shown in Fig. 9. Li_2FeSiO_4 has multiple crystal structures [24]. The most reported are orthogonal structure (Pmn2₁) [1] and monoclinic structure (P2₁/n) [25]. By comparing with the standard graph and the related literature, we found that the characteristic peaks of those two structures are very close. A full refinement has been carried out which shows that the dominant crystal phase of the two samples is the monoclinic structure P2₁/n
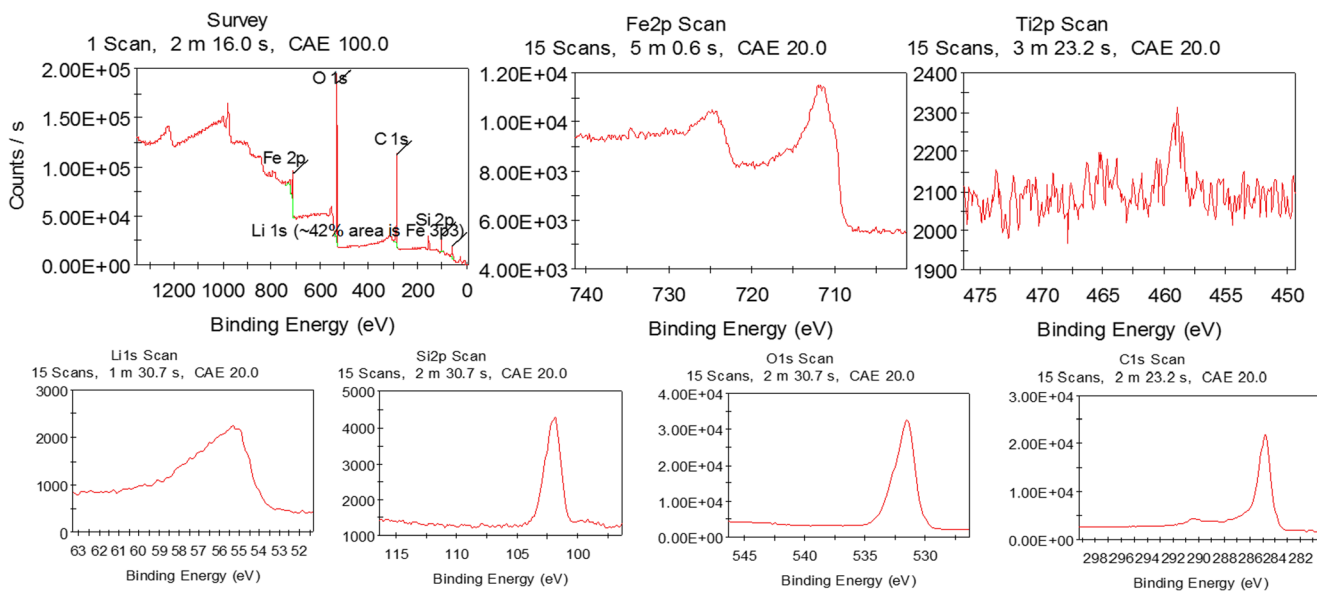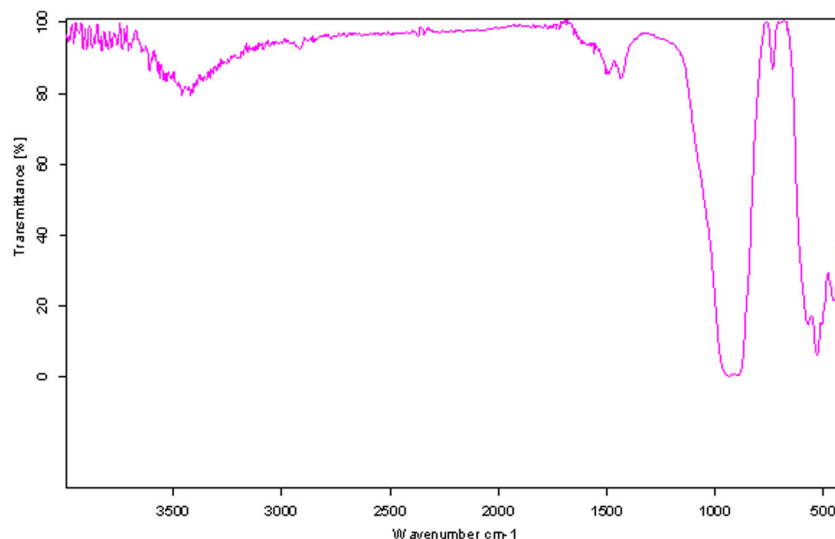

Fig. 12 XPS spectra of $Li_2FeSi_{0.98}Ti_{0.02}O_4$/C

Fig. 13 FT-IR spectra of $Li_2FeSi_{0.98}Ti_{0.02}O_4/C$

[10]. No diffraction peak (26°) of graphitized carbon crystallization can be found in these materials, which indicates that the carbon in the materials synthesized by the solid-state method exists in the form of amorphous state [26].

Figure 9 indicates that the doping metal is different, but the locations of the main peaks are similar. There are a few $Li_2Fe_3O_4$ peaks in the figure; the impurity peak of $Li_2FeSi_{0.98}Ag_{0.02}O_4/C$ is at 42.8°. The impurity peak of $Li_2Fe_3O_4$ does not exist in $Li_2FeSi_{0.98}Ti_{0.02}O_4/C$, which indicates that the purity of this material is high. The XRD spectrum shows that there are no characteristic peaks of Fe and Li_2SiO_3. Table 4 shows the lattice parameters of those two materials. The lattice volumes of $Li_2FeSi_{0.98}Ti_{0.02}O_4/C$ and $Li_2FeSi_{0.98}Ag_{0.02}O_4/C$ are larger than those of pure phase materials [35]. To sum up, the crystal structure of Li_2FeSiO_4 has not been changed after metal doping and the increase of the lattice volume can improve the pathway for the diffusion of lithium ion [27]. As a result, the electrochemical properties have been improved.

The SEM images of $Li_2FeSi_{0.98}Ti_{0.02}O_4/C$ and $Li_2FeSi_{0.98}Ag_{0.02}O_4/C$ are shown in Fig. 10 which indicate that the particle sizes of those two kinds of cathode materials are even and there is no obvious agglomeration phenomenon, which demonstrates that metal ion doped in the Si site could effectively inhibit the agglomeration of Li_2FeSiO_4 crystal, reduce the particle size, and shorten the diffusion distance of lithium ion. Metal ions doped into the crystal can reduce the negative effect on lithium ion moving in the crystal due to the strong bond of the Si–O. Consequently, the electrochemical properties of Li_2FeSiO_4 can be improved effectively via metal ions doped at the Si site because of the smooth movement and short diffusion distance of the lithium ion. The surface of the material is covered with amorphous carbon. The particles are cross-linked, the boundary of the particles is clear, the edges are smooth, and there are small spherical particles. It indicates

that the materials have a high specific surface area. Carbon coating can prevent particle agglomeration, shorten the diffusion path of lithium ion, and provide a good electron transport channel for lithium-ion deintercalation [28–30]. The particle size of $Li_2FeSi_{0.98}Ti_{0.02}O_4/C$ is smaller and the distribution is uniform. A few agglomeration particles can be observed in $Li_2FeSi_{0.99}Ag_{0.01}O_4/C$, which is consistent with the test results of the cyclic performance and the capacity of the materials.

According to the analysis above, the properties of $Li_2FeSi_{0.98}Ti_{0.02}O_4/C$ are the best. Then, $Li_2FeSi_{0.98}Ti_{0.02}O_4/C$ was tested by EDS, XPS, and FT-IR spectra. Figure 11 shows the EDS analysis of $Li_2FeSi_{0.98}Ti_{0.02}O_4/C$ which indicates that Fe, Si, O, and C elements are detected and the existence of Ti element has also been confirmed. Due to the limits of the detection range, the Be window of the detector blocks the X-ray from the Li element. Therefore, the content of Li could not be detected by EDS spectra. The proportion of Fe:Si:Ti is 0.989:1:0.017, which is close to the theoretical value. Even when using the high-rate electron microscope, it is difficult to get the average content of the whole material by measuring any point at random on the surface of the material, and the result is very difficult to accord exactly with the average content of the whole material. The above results show that the elements are uniformly distributed on the microscale. The test results for ICP are shown in Table 5. It can be seen from the test results that the molar ratio of each element of $Li_2FeSi_{0.98}Ti_{0.02}O_4/C$ is very close to the feed ratio, which meets the requirement of stoichiometric ratio.

XPS is used to explore the composition and chemical valence state of elements in $Li_2FeSi_{0.98}Ti_{0.02}O_4/C$. The results are shown in Fig. 12. The spectrum scanning of XPS shows that there are characteristic peaks of Li, Fe, Si, O, and C elements in the samples [31]; that is, the characteristic peaks of Li 1s, Fe 2p, Si 2p, O 1s, and C 1s. From Fig. 12, we can

observe the XPS spectra of Fe2p. The characteristic peak located in 711.38 eV of $Li_2FeSi_{0.98}Ti_{0.02}O_4$/C is consistent with $Fe2p_{3/2}$ and $Fe2p_{1/2}$ of Fe^{2+} which has been reported in literature [32]. Therefore, the ferric ions in $Li_2FeSi_{0.98}Ti_{0.02}O_4$/C are Fe^{2+}. The XPS spectrum of C1s is 285.02 eV. The peaks correspond to C=C [33]. The existence of C=C bond indicates that the material contains carbon. In $Li_2FeSi_{0.98}Ti_{0.02}O_4$/C samples, the characteristic peaks of Ti2p are observed at 458.8 eV, which is consistent with the binding energies of Ti^{4+} [34]. The results of XPS show that the existence of Ti elements is not only on the surface of the material, but also in the material. It is confirmed that Ti^{4+} has succeeded in replacing Si^{4+} into the lattice of Li_2FeSiO_4.

Figure 13 shows the FT-IR spectra of $Li_2FeSi_{0.98}Ti_{0.02}O_4$/C. All the peaks in Fig. 13 come from the vibration of the inner group. The characteristic absorption peaks of Li_2FeSiO_4 materials are mainly composed of Li–O, Si–O, and Fe–O. The locations of the absorption peaks in Fig. 13 are basically consistent with those reported in literature [35]. The characteristic peaks in 893.33 cm^{-1} and 529.42 cm^{-1} of $Li_2FeSi_{0.98}Ti_{0.02}O_4$/C correspond to the tensile and bending vibration of Si–O in SiO_4^{4-}. However, the characteristic peaks of Si–O in $LiSiO_3$ are located in 1100 cm^{-1} and 780 cm^{-1} [36, 37], which are not observed in $Li_2FeSi_{0.98}Ti_{0.02}O_4$/C. Combined with XRD analysis, there is no $LiSiO_3$ in the samples. The characteristic peak in 448.73 cm^{-1} of $Li_2FeSi_{0.98}Ti_{0.02}O_4$/C corresponds to the tensile and bending vibration of LiO_4. The absorption peak of the Fe–O bond is below 400 cm^{-1}, which cannot be observed in the figure. The positions of the absorption peaks in the figure are basically consistent with those reported in literature [38, 39], which indicates that $Li_2FeSi_{0.98}Ti_{0.02}O_4$/C has been synthesized.

Conclusions

$Li_2FeSi_{0.98}M_{0.02}O_4$/C (M = Ti, Ag, Cu, V, and Pb) was synthesized by the solid-state method, and the electrochemical performance tests were carried out. By comparing the electrochemical properties of $Li_2FeSi_{1-x}M_xO_4$/C (M = Ti, Ag; x = 0.01, 0.02, 0.03, 0.05), we could conclude that $Li_2FeSi_{0.98}Ti_{0.02}O_4$/C and $Li_2FeSi_{0.98}Ag_{0.02}O_4$/C have better discharge capacity. The initial discharge capacity of $Li_2FeSi_{0.98}Ti_{0.02}O_4$/C is 164.1 mAh/g, which is equivalent to 0.98 Li^+ deintercalation. The capacity of $Li_2Fe_{0.98}Ti_{0.02}SiO_4$/C is 155.8 mAh/g after 10 cycles under 0.1 C, and the capacity retention rate is 94.9%. The initial discharge capacity of $Li_2FeSi_{0.98}Ag_{0.02}O_4$/C is 166.6 mAh/g, which is better than that of other materials. The capacity of $Li_2Fe_{0.98}Ag_{0.02}SiO_4$/C is 132.8 mAh/g after 10 cycles under 0.1 C, and the capacity retention rate is 79.7%. The charge/discharge cycle performance of $Li_2FeSi_{0.98}Ti_{0.02}O_4$/C is more stable than $Li_2FeSi_{0.98}Ag_{0.02}O_4$/C and other materials as well. The

diffusion coefficient of lithium ion of $Li_2FeSi_{0.98}Ti_{0.02}O_4$/C is higher than that of pure phase material by two orders of magnitude. The XRD patterns show that the dominant crystal phase of the samples is the monoclinic structure $P2_1/n$ and there are no characteristic peaks of impurities such as Fe or Li_2SiO_3 in the materials, which indicate that the crystal structure of Li_2FeSiO_4 has not been changed after doping metal ion at the silicon site. The SEM shows that the particle size of $Li_2FeSi_{0.98}Ti_{0.02}O_4$/C is the smallest and its distribution is uniform. EDS analysis indicates that the elements are uniformly distributed on the microscale. It can be seen from the ICP test results that the molar ratio of each element of $Li_2FeSi_{0.98}Ti_{0.02}O_4$/C is very close to the feed ratio, which meets the requirement of stoichiometric ratio. The XPS spectrum has confirmed that Ti^{4+} has succeeded in replacing Si^{4+} into the lattice of Li_2FeSiO_4. The location of each absorption peak in the infrared spectrogram is the same as reported in the literature, which shows that stable materials are formed.

References

1. Liivat A (2012) Structural changes on cycling Li_2FeSiO_4 polymorphs from DFT calculations. Solid State Ionics 228:19–24
2. Zaghib K, Salah AA, Ravet N et al (2006) Structural, magnetic and electrochemical properties of lithium iron orthosilicate. J Power Sources 160(2):1381–1386
3. Nytén A, Abouimrane A, Armand M, Gustafsson T, Thomas JO (2005) Electrochemical performance of Li_2FeSiO_4 as a new Li-battery cathode material. Electrochem Commun 7(2):156–160
4. Yan Z, Cai S, Miao L, Zhou X, Zhao Y (2012) Synthesis and characterization of in situ carbon-coated Li_2FeSiO_4 cathode materials for lithium ion battery. J Alloys Compd 511(1):101–106
5. Qu L, Fang S, Yang L, Hirano SI (2012) Li_2FeSiO_4/C cathode material synthesized by template-assisted sol-gel process with Fe_2O_3 microsphere. J Power Sources 217:243–247
6. Oghbaei M, Baniasadi F, Asgari S (2016) Lithium iron silicate sol-gel synthesis and electrochemical investigation. J Alloys Compd 672:93–97
7. Xu Y, Shen W, Zhang A, Liu H, Ma Z (2014) Template-free hydrothermal synthesis of Li_2FeSiO_4 hollow spheres as cathode materials for lithium-ion batteries. J Mater Chem A 2(32):12982–12990
8. Zhang M, Chen Q, Xi Z, Hou Y, Chen Q (2012) One-step hydrothermal synthesis of Li_2FeSiO_4/C composites as lithium-ion battery cathode materials. J Mater Sci 47(5):2328–2332
9. Ren B, Xu Y, Yang R et al (2009) Preparation of Li_2FeSiO_4 as cathode materials for Lithium-ion battery by solid-state reaction. Mater Heat Treatment 38:41–43
10. Zhang S, Deng C, Yang S (2009) Preparation of nano-Li_2FeSiO_4 as cathode material for lithium-ion batteries. Electrochem Solid-State Lett 12(7):A136–A139
11. Gong ZL, Li YX, He GN, Li J, Yang Y (2008) Nanostructured Li_2FeSiO_4 electrode material synthesized through hydrothermal-assisted sol-gel process. Electrochem Solid-State Lett 11(5):A60–A63

12. Zheng Z, Wang Y, Zhang A, Zhang T, Cheng F, Tao Z, Chen J (2012) Porous Li_2FeSiO_4/C nanocomposite as the cathode material of lithium-ion batteries. J Power Sources 198:229–235

13. Gao K (2014) Effect of Mn doping on electrochemical properties of Li_2FeSiO_4/C cathode materials based on a vacuum solid-state method. Ionics 20(6):809–815

14. Zhang Z, Liu X, Wu Y, Zhao H, Chen B, Xiong W (2015) Synthesis and characterization of spherical $Li_2Fe_{0.5}V_{0.5}SiO_4$/C composite for high-performance cathode material of Lithium-ion secondary batteries. J Electrochem Soc 162(4):A737–A742

15. Deng C, Zhang S, Yang SY, Fu BL, Ma L (2011) Synthesis and characterization of $Li_2Fe_{0.97}M_{0.03}SiO_4$ (M= Zn^{2+}, Cu^{2+}, Ni^{2+}) cathode materials for lithium ion batteries. J Power Sources 196(1): 386–392

16. Zhang S, Deng C, Fu BL et al (2010) Doping effects of magnesium on the electrochemical performance of Li_2FeSiO_4 for lithium ion batteries. J Electroanal Chem 644(2):150–154

17. Zhang S, Deng C, Fu BL et al (2010) Effects of Cr doping on the electrochemical properties of Li_2FeSiO_4 cathode material for lithium-ion batteries. Electrochim Acta 55(28):8482–8489

18. Chen M, Shi J, Zhang Y et al (2011) Desorption of microscale silicone from concentrated hydrochloric acid by the adsorption method. J Jilin Inst Chem Technol 28(5):10–14

19. Armand M, Tarascon JM, Arroyo-de Dompablo ME (2011) Comparative computational investigation of N and F substituted polyoxoanionic compounds: the case of Li_2FeSiO_4 electrode material. Electrochem Commun 13(10):1047–1050

20. Chen J (2013) Recent progress in advanced materials for lithium ion batteries. Materials 6(1):156–183

21. Li L, Han E, Yang P, Zhu L, Liu Y (2018) Study on electrochemical performance of Mg-doped Li_2FeSiO_4 cathode material for Li-ion batteries. Ionics 24(7):1869–1878

22. Shao B, Taniguchi I (2012) Synthesis of Li_2FeSiO_4/C nanocomposite cathodes for lithium batteries by a novel synthesis route and their electrochemical properties. J Power Sources 199:278–286

23. Liu S, Xu J, Li D, Hu Y, Liu X, Xie K (2013) High capacity Li_2MnSiO_4/C nanocomposite prepared by sol-gel method for lithium-ion batteries. J Power Sources 232:258–263

24. Boulineau A, Sirisopanaporn C, Dominko R, Armstrong AR, Bruce PG, Masquelier C (2010) Polymorphism and structural defects in Li_2FeSiO_4. Dalton Trans 39(27):6310–6316

25. Nishimura S, Hayase S, Kanno R et al (2008) Structure of Li_2FeSiO_4. J Am Chem Soc 130(40):13212–13213

26. Jeon IY, Shin YR, Sohn GJ, Choi HJ, Bae SY, Mahmood J, Jung SM, Seo JM, Kim MJ, Wook Chang D, Dai L, Baek JB (2012) Edge-carboxylated graphene nanosheets via ball milling. Proc Natl Acad Sci 109(15):5588–5593

27. Tarascon JM, Armand M (2001) Issues and challenges facing rechargeable lithium batteries. Nature 414:359–367

28. Aravindan V, Karthikeyan K, Kang KS, Yoon WS, Kim WS, Lee YS (2011) Influence of carbon towards improved lithium storage properties of Li_2MnSiO_4 cathodes. J Mater Chem 21(8):2470–2475

29. Kempaiah DM, Rangappa D, Honma I (2012) Controlled synthesis of nanocrystalline Li_2MnSiO_4 particles for high capacity cathode application in lithium-ion batteries. Chem Commun 48(21):2698–2700

30. Bhaskar A, Deepa M, Rao TN, Varadaraju UV (2012) In situ carbon coated Li_2MnSiO_4/C composites as cathodes for enhanced performance Li-ion batteries. J Electrochem Soc 159(12):A1954–A1960

31. Zhang LL, Sun HB, Yang XL, Wen YW, Huang YH, Li M, Peng G, Tao HC, Ni SB, Liang G (2015) Study on electrochemical performance and mechanism of V-doped Li_2FeSiO_4 cathode material for Li-ion batteries. Electrochim Acta 152:496–504

32. Gao H, Hu Z, Zhang K, Cheng F, Chen J (2013) Intergrown $Li_2FeSiO_4·LiFePO_4$-C nanocomposites as high-capacity cathode materials for lithium-ion batteries. Chem Commun 49(29):3040–3042

33. Mao M, Jiang L, Wu K et al (2015) The structure control of Zn/S graphene composites and their excellent properties for lithium-ion batteries. J Mater Chem A 3(25):13384–13389

34. Zhang Y, Du F, Yan X et al (2014) Improvements in the electrochemical kinetic properties and rate capability of anatase titanium dioxide nanoparticles by nitrogen doping. ACS Appl Mater Interfaces 6(6):4458–4465

35. Guo HJ, Xiang K, Cao X et al (2009) Preparation and characteristics of Li_2FeSiO_4/C composite for cathode of lithium ion batteries. Trans Nonferrous Metals Soc China 19(1):166–169

36. Chen Z, Qiu S, Cao Y, Qian J, Ai X, Xie K, Hong X, Yang H (2013) Hierarchical porous Li_2FeSiO_4/C composite with 2 Li storage capacity and long cycle stability for advanced Li-ion batteries. J Mater Chem A 1(16):4988–4992

37. Lv D, Wen W, Huang X, Bai J, Mi J, Wu S, Yang Y (2011) A novel Li_2FeSiO_4/C composite: synthesis, characterization and high storage capacity. J Mater Chem 21(26):9506–9512

38. Fergus JW (2010) Recent developments in cathode materials for lithium ion batteries. J Power Sources 195(4):939–954

39. Li L, Han E, Dou L, Zhu L, Mi C, Li M, Niu J (2018) Enhanced electrochemical performance of Li_2FeSiO_4/C as cathode for lithium-ion batteries via metal doping at Fe-site. Solid State Ionics 325:30–42